

# Nonlinear Spin Polarized Transport Through a Quantum Dot

Baigeng Wang<sup>1</sup>, Jian Wang<sup>1</sup> and Hong Guo<sup>2</sup>

1. Department of Physics, The University of Hong Kong,  
Pokfulam Road, Hong Kong, China

2. Center for the Physics of Materials and Department  
of Physics, McGill University, Montreal, PQ, Canada H3A 2T8

We present a theoretical analysis of the nonlinear bias and temperature dependence of current-voltage characteristics of a spin-valve device which is formed by connecting a quantum dot to two ferromagnetic electrodes whose magnetic moments orient at an angle  $\theta$  with respect to each other. The theory is based on nonequilibrium Green's function approach and focused on current perpendicular to plane geometry. Coulomb interaction has been taken into account explicitly at the Hartree level. We derive a formula in closed form for current flowing through the device in general terms of bias and temperature. In the wideband limit we report exact results for the TMR junction nonlinear I-V curve as a function of  $\theta$ . We also report the conductance slope at zero bias as a function of temperature for which experimental results reported an anomalous behavior.

73.23.Ad,73.40.Gk,72.10.Bg

## I. INTRODUCTION

Due to the exciting perspective of magnetoelectronics where coherent charge and polarized spin are both utilized for electronic device functions<sup>1</sup>, quantum transport properties of systems with a magnetic character have attracted extensive attention. The well known giant magnetoresistance effect (GMR) is such a spin-polarized electronic transport effect<sup>2,3</sup>, using which a GMR device changes its resistance depending on the orientation of magnetic moments of the magnetic multi-layers forming the device. A GMR system is fabricated by sandwiching non-magnetic metal layer between two magnetic layers<sup>2</sup>, and further extensions or variations of this structure can produce many other device functions, including the spin-valve transistor<sup>4</sup>, spin selective electron interferometer<sup>5</sup>, and nonvolatile RAM<sup>6</sup>. While GMR is perhaps one of the most fruitful areas of fundamental research which has already produced substantial application with huge commercial value, an entirely different approach, also exploiting spin-polarized transport, is the tunneling magnetoresistance (TMR) where an insulating (I) material layer is sandwiched in between two ferromagnetic (FM) layers<sup>7</sup>, forming a *FM/I/FM* structure. One important attraction of a TMR device is that it carries lower current than the metallic GMR system, hence TMR can be, in principle, more advantageous for portable devices. Due to the reported room temperature operation of TMR<sup>8</sup>, the fundamental principle and various transport charac-

teristics of TMR devices have been the subject of increasingly more research, and will be the topic of the present work.

Tunneling of spin-polarized electrons through the TMR structure gives a large tunneling magnetoresistance (TMR) through the spin-valve effect<sup>7,9</sup>. The spin valve effect is characterized by the fractional change of resistance  $\kappa \equiv \Delta R/R$ , where  $\Delta R$  is the difference in resistance when magnetization of the two ferromagnetic metals are in parallel or anti-parallel. In the original experiment of Julliere on *Co/Ge/Fe*,  $\kappa$  was determined to be about 14% at 4.2K temperature at zero external bias voltage, and it dropped to 1% when bias was increased to a few meV. More recently, large TMR was reported<sup>8,10</sup> to persist at room temperature where  $\kappa$  is about 11.8% for *CoFe/Al<sub>2</sub>O<sub>3</sub>/Co* at small bias. Again, in this device  $\kappa$  decreases drastically when the voltage increases<sup>8,10</sup>. These experimental results clearly point to the need of a thorough theoretical understanding of the bias as well as temperature dependence of TMR. On the theoretical side, TMR has been investigated by many authors. Zhang *et.al.* have considered<sup>11</sup> TMR using a transfer matrix and calculated the tunnel conductance and magnetoresistance of a FM/I/FM system with an oscillatory but decaying bias voltage dependence of TMR resulting from quantum resonance. Bratkovsky<sup>12</sup> investigated a similar system and compared cases with or without impurity scattering. Barnaś and Fert investigated magnetoresistance oscillations due to charging effects<sup>13</sup>; Zhang *et.al.*<sup>14</sup> investigated the zero-bias anomaly of the experimental data<sup>8</sup> and provided an explanation that the anomaly is due to localized spin excitations at the barrier-electrode interface; and a number of studies<sup>11,12,15-17</sup> were devoted to improve the original TMR model of Julliere<sup>7</sup>. Very recently, the nonlinear bias dependence of an interesting TMR device in the form of *FM/I/FM/I/FM* was investigated theoretically<sup>18</sup>. Due to the relative magnetic moment orientation of the three FM layers as well as the quantum well formed by the two insulating layers, various very interesting TMR behavior can be expected<sup>18</sup>.

The purpose of this work is to further investigate TMR effect as a function of external bias as well as temperature in a *FM/I/FM* device structure, where we pay special attention to the internal Coulomb potential due to interactions. For a quantum device subjected to an external bias voltage, the internal potential build-up can be an important factor determining transport characteristics at

the nonlinear regime<sup>19</sup>, and this has not been included in previous analysis Ref. 11,12,18,14 of the bias dependence of TMR. There, external bias potentials are included non-self-consistently through Fermi functions of the electron reservoirs. In this paper we present a theory for TMR junctions based on the nonequilibrium Green's function, where the internal potential is solved self-consistently at the Hartree level. In particular we derive a general expression for the electric current flowing through the TMR device in terms of external bias, temperature, and the angle  $\theta$  between the magnetic moments of the two FM electrodes. Due to the inclusion of the internal Coulomb potential into the theory, the predicted results are gauge invariant against the shift of the external bias — which is a fundamental requirement of any transport theory. In the wideband limit and applying the charging model for the internal potential, we further derive an analytic expression of angular dependence of the I-V curve at zero temperature. The temperature dependence of TMR is then studied via a numerical integration of our analytical formula. Finally, in the weakly nonlinear regime our theory allows predictions of the slope of the TMR near zero bias, where experiments<sup>8</sup> showed a dip of magnetoconductance at low temperatures. Our results showed that the slope smoothly crosses over from a finite value at low temperature to zero at high temperature.

The rest of this paper is organized as follows. In section II, we present the general theory by deriving a current expression for TMR junctions. In section III, we apply this current expression for various situations, and a summary is given in section IV.

## II. GENERAL THEORETICAL FORMULATION

The TMR device we examine is schematically shown in the inset of Fig. (1a). It consists of a quantum dot connected by two ferromagnetic electrodes to the outside world. The magnetic moment  $\mathbf{M}$  of the left electrode is pointing to the  $z$ -direction, the electric current is flowing in the  $y$ -direction, while the moment of the right electrode is at an angle  $\theta$  to the  $z$ -axis in the  $x - z$  plane. In second quantized form this device is described by the following Hamiltonian,

$$H = H_L + H_R + H_{dot} + H_T \quad (1)$$

where  $H_L$  and  $H_R$  describe the left and right electrodes where a DC bias potential is applied,

$$H_L = \sum_{k\sigma} (\epsilon_{kL} + \sigma M) c_{kL\sigma}^\dagger c_{kL\sigma} \quad (2)$$

$$H_R = \sum_{k\sigma} [(\epsilon_{kR} + \sigma M \cos \theta) c_{kR\sigma}^\dagger c_{kR\sigma} + M \sin \theta [c_{kR\sigma}^\dagger c_{kR\bar{\sigma}}] . \quad (3)$$

In Eq. (1),  $H_{dot}$  describes the quantum dot

$$H_{dot} = \sum_{n\sigma} \epsilon_n d_{n\sigma}^\dagger d_{n\sigma} . \quad (4)$$

$H_T$  models the coupling between electrodes and the quantum dot region (the scattering region) with hopping matrix  $T_{k\alpha n}$ . For simplicity we shall assume the hopping matrix to be independent of spin index, thus

$$H_T = \sum_{k\alpha n} [T_{k\alpha n} c_{k\alpha\sigma}^\dagger d_{n\sigma} + c.c.] . \quad (5)$$

In these expressions  $\epsilon_{k\alpha} = \epsilon_k^0 + qV_\alpha$  with  $\alpha = L, R$ ;  $c_{k\alpha\sigma}^\dagger$  (with  $\sigma = \uparrow, \downarrow$  or  $\pm 1$  and  $\bar{\sigma} = -\sigma$ ) is the creation operator of electrons with spin index  $\sigma$  inside the  $\alpha$ -electrode. Similarly  $d_{n\sigma}^\dagger$  is the creation operator of electrons with spin  $\sigma$  at energy level  $n$  for the quantum dot region. In writing down Eqs.(2) and (3), we have made a simplification that the value of molecular field  $M$  is the same for the two electrodes, thus the spin-valve effect is obtained<sup>9</sup> by varying the angle  $\theta$ . Essentially,  $M$  mimics the difference of density of states (DOS) between spin up and down electrons<sup>9</sup> in the electrodes. Finally, due to electron-electron interactions an internal potential build-up  $U(\mathbf{r})$  is induced inside the quantum dot region. Hence the actual Hamiltonian of the quantum dot is  $H_{dot} + qU$ .

To proceed, we first apply the following Bogoliubov transformation<sup>20</sup> to diagonalize the Hamiltonian of the right electrode,

$$c_{kR\sigma} \rightarrow \cos(\theta/2)C_{kR\sigma} - \sigma \sin(\theta/2)C_{kR\bar{\sigma}} \quad (6)$$

$$c_{kR\sigma}^+ \rightarrow \cos(\theta/2)C_{kR\sigma}^+ - \sigma \sin(\theta/2)C_{kR\bar{\sigma}}^+ \quad (7)$$

from which we obtain the effective Hamiltonian

$$H_\alpha = \sum_{k\sigma} [(\epsilon_{k\alpha} + \sigma M) C_{k\alpha\sigma}^\dagger C_{k\alpha\sigma} \quad (8)$$

$$H_T = \sum_{kn\sigma} [T_{kLn\sigma} C_{kL\sigma}^\dagger d_{n\sigma} + T_{kRn\sigma} (\cos \frac{\theta}{2} C_{kR\sigma}^\dagger - \sigma \sin \frac{\theta}{2} C_{kR\bar{\sigma}}^\dagger) d_{n\sigma} + c.c.] . \quad (9)$$

The electric current flowing the TMR device modeled by Eqs. (1, 8, 4, 9) can be written, following the derivations of Ref. 21 and extending it to include spin dependent scattering, in terms of the Green's functions of the quantum dot ( $\hbar = 1$ ),

$$I_\alpha = iq \int (dE/\pi) Tr \{ -2Im(\Sigma_\alpha^r) \times [(\mathbf{G}^r - \mathbf{G}^a) f_\alpha + \mathbf{G}^<] \} \quad (10)$$

where  $f_\alpha \equiv f(E - qV_\alpha)$  and the trace is over both the state index and spin index. Here  $\mathbf{G}^r(E, U)$  is the

$2 \times 2$  matrix in spin space for the retarded Green's function with  $U(\mathbf{r})$  the electro-static potential build-up inside quantum dot region. In Hartree approximation  $\mathbf{G}^r(E, U)$  is given by

$$\mathbf{G}^r(E, U) = \frac{1}{E - H_{dot} - qU - \Sigma^r} \quad (11)$$

where the self-energy  $\Sigma^r \equiv \Sigma_L^r(E - qV_L) + \Sigma_R^r(E - qV_R)$  is also a  $2 \times 2$  matrix in spin space, which describes coupling of the quantum dot region to the two magnetic electrodes. The detailed analysis of self-energy is given in the Appendix and the result is written as

$$\Sigma_\alpha^r(E) = \hat{R}_\alpha \begin{pmatrix} \Sigma_{\alpha\uparrow}^r & 0 \\ 0 & \Sigma_{\alpha\downarrow}^r \end{pmatrix} \hat{R}_\alpha^\dagger \quad (12)$$

with the rotational matrix  $\hat{R}_\alpha$  for electrode  $\alpha$  defined as

$$\hat{R} = \begin{pmatrix} \cos \theta_\alpha/2 & \sin \theta_\alpha/2 \\ -\sin \theta_\alpha/2 & \cos \theta_\alpha/2 \end{pmatrix} \quad (13)$$

Here angle  $\theta_\alpha$  is defined as  $\theta_L = 0$  and  $\theta_R = \theta$  and  $\Sigma_{\alpha\sigma}^r$  is given by

$$\Sigma_{\alpha\sigma mn}^r = \sum_k \frac{T_{k\alpha m}^* T_{k\alpha n}}{E - \epsilon_{k\alpha\sigma} + i\delta} \quad (14)$$

The lesser Green's function  $\mathbf{G}^<$  in Eq. (10) is calculated<sup>21</sup> through the Keldysh equation  $\mathbf{G}^< = \mathbf{G}^r \mathbf{G}^< \mathbf{G}^a$  with the self energy  $\Sigma^< = \Sigma_L^<(E - qV_L) + \Sigma_R^<(E - qV_R)$  given by the following expression at equilibrium,

$$\Sigma_\alpha^<(E) = i f_\alpha \hat{R}_\alpha \begin{pmatrix} \Gamma_{\alpha\uparrow} & 0 \\ 0 & \Gamma_{\alpha\downarrow} \end{pmatrix} \hat{R}_\alpha^\dagger \quad (15)$$

where  $\Gamma_{\alpha\sigma} = -2Im(\Sigma_{\alpha\sigma}^r)$  is the linewidth function.

Using Keldysh equation and the explicit self-energy expressions (12,15), after tedious but straightforward manipulations one can confirm that Eq.(10) becomes

$$I_\alpha = \frac{2q}{\pi} \int dE \sum_{\beta \neq \alpha} Tr [Im(\Sigma_\alpha^r) \mathbf{G}^r Im(\Sigma_\beta^r) \mathbf{G}^a] (f_\alpha - f_\beta) \quad (16)$$

Note that the same form of current expression is true for systems without spin dependent scattering<sup>22</sup>. But with such scattering, the trace is over states as well as spin variables. Eq. (16) is the basis for our further analysis.

Before presenting the results for the Green's function  $\mathbf{G}^r$ , it is worth to emphasize that it is now explicitly dependent on the internal potential landscape through the Hartree potential  $U(\mathbf{r})$ . This is an extension to the previous NEGF analysis<sup>21,23,24</sup> and it allows us to investigate TMR within gauge invariance requirement. At Hartree level  $U(\mathbf{r})$  is determined by the self-consistent Poisson equation

$$\nabla^2 U = 4\pi iq \int (dE/2\pi) \sum_\sigma (\mathbf{G}^<(E, U))_{\sigma\sigma} \quad (17)$$

Eq. (17) is a *nonlinear* equation because  $\mathbf{G}^{r,a}$  depends on  $U(\mathbf{r})$  by Eq.(11). Hence in this theory there is a need to self-consistently solve the coupled equations of  $\mathbf{G}^{r,a}$  and  $U(\mathbf{r})$ . This presents some analytical difficulties (see next section).

Eqs. (16,11,17) completely determine the nonlinear I-V characteristics of multi-probe TMR junctions. It is not difficult to directly prove that the current expression Eq.(16) is gauge invariant: shifting the potential at all the electrodes by a constant  $\Delta V$ ,  $V_\alpha \rightarrow V_\alpha + \Delta V$ ,  $I_\alpha$  from Eq. (16) remains the same.

From now on we focus on the two-probe TMR device of the inset of Fig. (1a) for which  $I_L = -I_R = I$ . After expanding the spin part of the trace in Eq. (16), we obtain the final expression of electric current for the TMR device,

$$I = \frac{q}{2\pi} \int dE Tr [ \begin{aligned} & \Gamma_{L\uparrow} G_{11}^r (\Gamma_{R\uparrow} \cos^2 \frac{\theta}{2} + \Gamma_{R\downarrow} \sin^2 \frac{\theta}{2}) G_{11}^a \\ & - \Gamma_{L\uparrow} G_{12}^r (2\Gamma_{L\downarrow} + \Gamma_{R\downarrow} \cos^2 \frac{\theta}{2} + \Gamma_{R\uparrow} \sin^2 \frac{\theta}{2}) G_{12}^a \\ & - \Gamma_{L\downarrow} G_{21}^r (2\Gamma_{L\uparrow} + \Gamma_{R\uparrow} \cos^2 \frac{\theta}{2} + \Gamma_{R\downarrow} \sin^2 \frac{\theta}{2}) G_{21}^a \\ & + \Gamma_{L\downarrow} G_{22}^r (\Gamma_{R\downarrow} \cos^2 \frac{\theta}{2} + \Gamma_{R\uparrow} \sin^2 \frac{\theta}{2}) G_{22}^a \end{aligned} ] (f_R - f_L) \quad (18)$$

In this result, the  $2 \times 2$  Green's function matrix  $\mathbf{G}^r$  is determined by the usual method of equation of motion<sup>21</sup>. For our Hamiltonian the equation of motion can be solved exactly through straightforward algebra, and they are found to be:

$$G_{11}^r \equiv G_{\uparrow\uparrow}^r = \frac{A_\downarrow}{A_\uparrow A_\downarrow - B^2} \quad (19)$$

$$G_{12}^r \equiv G_{\uparrow\downarrow}^r = G_{21}^r \equiv G_{\downarrow\uparrow}^r = \frac{B}{A_\uparrow A_\downarrow - B^2} \quad (20)$$

$$G_{22}^r \equiv G_{\downarrow\downarrow}^r = \frac{A_\uparrow}{A_\uparrow A_\downarrow - B^2} \quad (21)$$

where  $A_\sigma$  and  $B$  are defined as

$$A_\sigma = E - H_{dot} - qU - \Sigma_\sigma^r \quad (22)$$

$$B = \frac{i}{2} (\Gamma_{R\downarrow} - \Gamma_{R\uparrow}) \sin \frac{\theta}{2} \cos \frac{\theta}{2} \quad (23)$$

Before finishing this section, we note that Eqs. (18, 19, 20, 21, 17) form the basis for numerical calculations of TMR I-V curves beyond what has been done before,

since it is a gauge invariant formula. In a typical numerical analysis, one computes Green's functions  $\mathbf{G}^r$  and the coupling matrix  $\Gamma$  using tight-binding models<sup>22</sup>; and the Poisson equation can be solved using very powerful numerical techniques<sup>25</sup>. Numerical analysis of these expressions is beyond the scope of this paper and in the next section we attempt to obtain the I-V characteristics via analytic means.

### III. APPLICATIONS

As discussed in the last section, the spin dependent nonlinear I-V characteristics of the TMR device is obtained by self-consistently solving Eqs. (18,19, 20, 21, 17). Due to complexity of this problem, some reasonable approximations need to be made. In particular we will present applications of our theory from two approximations. First, instead of solving the Poisson equation (17) for  $U(\mathbf{r})$  analytically which is perhaps impossible to do, we will parameterize  $U$  in terms of related geometrical capacitance. This is the discrete potential approximation commonly used in theoretical analysis<sup>26,24</sup>. This analysis allows us to calculate general nonlinear I-V curves at various temperature and qualitatively compare with the experimental observations. Second, at weakly nonlinear regime, the bias voltage is finite but small hence one can expand the entire current formula in terms of bias order by order. In this case the Poisson equation can be directly solved to yield a spatially varying  $U(\mathbf{r})$ . At weakly nonlinear regime, we calculate the second order nonlinear conductance which is the slope of the I-V curve at zero bias. Experimentally<sup>8</sup> one observes a finite slope at low temperature, while zero slope at high temperature.

#### A. TMR I-V curves and ratios

To obtain a general qualitative behavior of the I-V curves, we shall simplify the current formula (18) using the discrete potential approximation. In this approximation<sup>26,27</sup> one assumes that  $U(\mathbf{r}) = U_o$  is a constant that provides a shift to the band bottom of the quantum dot due to Coulomb interactions. To solve for  $U_o$ , we introduce geometrical capacitance coefficients  $C_1$  and  $C_2$  between the electrodes and the quantum dot. The total charge  $\Delta Q$  in the quantum dot is given by the right hand side of Eq. (17), and we parameterize  $\Delta Q$  using  $C_1$  and  $C_2$ ,

$$\begin{aligned} \Delta Q &= -\frac{i}{2\pi} \int dE Tr [\mathbf{G}^<(E, U_0) - \mathbf{G}_0^<] \\ &= C_1 \times (U_0 - V_1) + C_2 \times (U_0 - V_2) . \end{aligned} \quad (24)$$

Hence by evaluating the energy integration and using  $C_1$ ,  $C_2$  as input parameters, one obtains  $U_o$ .

The explicit expressions for the Green's functions and hence the current (18) and charge (24), can be derived in

the wideband limit<sup>21</sup> where the coupling matrix  $\Gamma$  is independent of energy. In this limit the energy integrations of (18, 24) can be completed. For instance, assuming  $\Gamma_{L\sigma} = \Gamma_{R\sigma} \equiv \Gamma_\sigma$ , at zero temperature we obtain the I-V curve of the TMR device to be,

$$I = \sum_\sigma p_\sigma \left( \arctan \frac{2E_1}{\Gamma + \sigma\Delta\Gamma \cos\theta/2} - \arctan \frac{2E_2}{\Gamma + \sigma\Delta\Gamma \cos\theta/2} \right) \quad (25)$$

where  $\Gamma = \Gamma_\uparrow + \Gamma_\downarrow$ ,  $\Delta\Gamma = \Gamma_\uparrow - \Gamma_\downarrow$ ,  $E_\alpha = E_F - E_0 - qU_0 + qV_\alpha$ , and

$$p_\sigma = -\frac{q}{4\pi\Gamma} (\Gamma^2 + \sigma\Gamma\Delta\Gamma \cos\frac{\theta}{2} - \Delta\Gamma^2 \sin^2\frac{\theta}{2}) .$$

The internal potential  $U_o$  is determined by the following equation obtained by evaluating the charge  $\Delta Q$  at the wideband limit,

$$\begin{aligned} &\sum_{\alpha\sigma} \left[ \arctan \frac{2E_\alpha}{\Gamma + \sigma\Delta\Gamma \cos\theta/2} \right. \\ &\quad \left. - \arctan \frac{2(E_F - E_0)}{\Gamma + \sigma\Delta\Gamma \cos\theta/2} \right] \\ &= \frac{2\pi}{q} [C_1(U_0 - V_1) + C_2(U_0 - V_2)] . \end{aligned} \quad (26)$$

To get physical insight we plot the I-V characteristics at different temperature parameter  $\beta$  and magnetic moment orientation  $\theta$ . We have chosen  $\Gamma_\uparrow = 1.0$ ,  $\Gamma_\downarrow = 0.4$ ,  $C_1 = C_2 = 0.5$  and  $E_F - E_0 = -2$  (units set by  $\hbar = e = 2m = 1$ ).

Fig.(1a) shows I-V curves at zero temperature  $\beta = \infty$  for different orientations  $\theta = 0$  (solid line),  $0.4\pi$  (dotted line), and  $0.8\pi$  (dashed line). Clearly current increases as the junction bias increases. When  $\theta = 0$ , *i.e.* when magnetic moment of the left and right electrodes are parallel, the current is largest at all bias voltages. When  $\theta = \pi$  for which the moments are anti-parallel, the current is the smallest. This is a well known result for TMR junctions at zero bias<sup>9</sup>, but it holds at finite bias as well. This behavior can be seen more clearly in Fig.(1b) where we plot current versus angle  $\theta$  at different bias  $\Delta V = (V_1 - V_2) = 2, 5, 8, 11, 14$ . For all cases  $I$  is minimum at  $\theta = \pi$ . When temperature is nonzero the energy integration of Eq. (18) cannot be completed analytically thus we integrate it numerically assuming phonons can be neglected. Fig. (2) plots current versus  $\theta$  at different temperatures  $\beta = 1, 0.5, 0.2$ . The current is sensitively dependent on temperature and decreases substantially when temperature is increased (smaller  $\beta$  corresponds to higher temperature). This is consistent with previous experimental findings<sup>7,8</sup>.

To calculate tunneling magnetoresistance ratio, we use the definition of Ref. 18 which defines a nonlinear resistance  $R = 1/G \equiv V/I$  and TMR ratio  $\equiv (R(0) -$

$R(\pi)/R(0)$ . The TMR ratio versus voltage is presented in Fig.(3) where two curves corresponding to  $\beta = \infty$  and  $\beta = 1$  are plotted respectively. At zero temperature, a large TMR ratio (about 30%) drops quickly as the voltage is increased, a trend agrees with experimental findings<sup>7,8</sup>. At small voltages, the TMR ratio is much lower for higher temperature, also in agreement with experimental results<sup>8</sup>. We note that the theoretical values of the TMR ratio, about 34% at low temperature, are much larger than the measured values<sup>10</sup> (about 27% at 77K), due to our choice of ideal model and system parameters. But the qualitative trend of these results are consistent. The TMR minimum in Fig. (3) is due to quantum resonance, as was also seen in previous studies<sup>11</sup>. Finally, we note that experimental data of TMR as a function of bias is a slight concave-shaped curve near zero bias, but that of our model, as well as of others<sup>12,11,18</sup>, are slightly convex. Thus the decay rate of TMR is faster in the measured data<sup>10</sup>, which indicates that other physical mechanisms<sup>14</sup> absent in the present model are perhaps needed to quantitatively understand the experimental data.

### B. Conductance dip at zero bias

Experimental results on TMR junctions of Ref. 8 showed that there is a clear conductance dip at zero bias at low temperature, a slight dip at intermediate temperature, and perhaps no dip at high temperature. This anomaly may be associated with a number of device details such as the presence of impurities, localization, and scattering. In this section we will examine the zero-bias conductance dip as a function of temperature.

The slope of conductance versus bias is the second order nonlinear conductance coefficient  $G_{\alpha\beta\gamma} \equiv d^2I_\alpha/dV_\beta dV_\gamma$  evaluated at zero bias voltages  $V_\beta \rightarrow 0$ ,  $V_\gamma \rightarrow 0$ . We apply a weakly nonlinear analysis of  $G_{\alpha\beta\gamma}$  in which all quantities of interest are expanded order by order in bias voltage. This way one can directly solve the Poisson equation (17) without using the discrete potential approximation: we seek the solution of  $U(\mathbf{r})$  in the following form,

$$U = U_{eq} + \sum_\alpha u_\alpha V_\alpha + \frac{1}{2} \sum_{\alpha\beta} u_{\alpha\beta} V_\alpha V_\beta + \dots \quad (27)$$

where  $U_{eq}$  is the equilibrium potential and  $u_\alpha(\mathbf{r})$ ,  $u_{\alpha\beta}(\mathbf{r})$  are the characteristic potentials<sup>19,28</sup>. It can be shown that the characteristic potential satisfy the following sum rules<sup>19,28</sup>  $\sum_\alpha u_\alpha = 1$  and  $\sum_\beta u_{\alpha\beta} = 0$ . Expanding  $\mathbf{G}^<$  of Eq. (17) in power series of  $V_\alpha$ , from the Poisson equation (17) one can derive equations for all the characteristic potentials. In particular the expansions are facilitated by Dyson equation to the appropriate order<sup>29</sup>:

$$\mathbf{G}^r = \mathbf{G}_0^r + \mathbf{G}_0^r (qU - qU_{eq}) \mathbf{G}_0^r + \dots$$

with  $\mathbf{G}_0^r$  the equilibrium retarded Green's function, *i.e.*, when  $U = U_{eq}$ . At the lowest order we obtain<sup>30</sup>

$$-\nabla^2 u_\alpha(\mathbf{r}) = -4\pi q^2 \frac{dn(\mathbf{r})}{dE} u_\alpha(\mathbf{r}) + 4\pi q^2 \frac{dn_\alpha(\mathbf{r})}{dE} \quad (28)$$

The first term on the right hand side of Eq. (28), which depends on internal potential  $u_\alpha$ , describes the induced charge density in the TMR junction. The second term of Eq.(28) is the *injectivity* which corresponds to the charge density due to external injection. Finally

$$\frac{dn_\alpha(x)}{dE} = -2 \sum_\sigma \int \frac{dE}{2\pi} (-\partial_E f) [\mathbf{G}_0^r Im \mathbf{\Sigma}_\alpha^r \mathbf{G}_0^a]_{\sigma\sigma} \quad (29)$$

and

$$\frac{dn}{dE} = \sum_\alpha \frac{dn_\alpha}{dE} \quad (30)$$

are the local density of states. Once the characteristic potential is obtained from Eq.(28), the the second order nonlinear spin dependent conductance  $G_{\alpha\beta\gamma}$  is given by

$$G_{\alpha\beta\gamma} = -\frac{2q^3}{2\pi} \int dE (-\partial_E f) Tr [(\mathbf{G}_0^a Im \mathbf{\Sigma}_\alpha^r \mathbf{G}_0^r \mathbf{G}_0^r + \mathbf{G}_0^a \mathbf{G}_0^a Im \mathbf{\Sigma}_\alpha^r \mathbf{G}_0^r) (Im \mathbf{\Sigma}^r \delta_{\alpha\gamma} - Im \mathbf{\Sigma}^r \delta_{\beta\gamma}) (2u_\beta - \delta_{\beta\gamma})] \quad (31)$$

where  $u_\beta$  in Eq.(31) is a  $2 \times 2$  diagonal matrix.

The conductance slope at zero bias which has been measured in the experiments of Ref. 8,10 is given by  $G_{111}$ , since  $G_{111}$  is the slope of  $dI/dV$  at zero bias. To simplify discussion we consider  $G_{111}$  near a resonant point where the Green's function is given by  $G_{0,11}^r = 1/(E_F - E_0 + i\Gamma_{\uparrow}/2)$  and  $G_{0,22}^r = 1/(E_F - E_0 + i\Gamma_{\downarrow}/2)$ . In addition, apply the quasi-neutrality approximation<sup>31</sup> we have  $u_1 = (dn_1/dE)/(dn/dE)$ . Thus expression (31) is easily calculated. In Fig. (4) we plot  $G_{111}$  as a function of temperature at  $E_F = 2.5$  while  $E_0 = 3.0$ . As the temperature is increased ( $\beta$  decreases),  $G_{111}$  goes to zero smoothly. Our model thus indicates that conductance slope  $G_{111}$  is nonzero at small temperature, and it diminishes to zero at high temperatures, consistent with experimental results<sup>8</sup>. Our result also indicates that the crossover from a finite slope to zero slope as a function of temperature is smooth, as shown in Fig. (4).

### IV. SUMMARY

In this paper, quantum transport properties of a mesoscopic conductor connected to two metallic ferromagnetic electrodes have been studied theoretically. We derived self-consistent equations which completely determine nonlinear I-V characteristics of the TMR device. Our theory is gauge invariant due to the inclusion of

long-range Coulomb potential. In the wideband limit the nonlinear I-V curves and the TMR ratio at different temperature and magnetic moment orientation  $\theta$  are calculated and our results are qualitatively consistent with the experimental measurements. We were also able to investigate the conductance slopes at zero bias for various temperatures, where experimental measurements showed an anomaly. Experimental measurements<sup>8</sup> gave data for a few temperatures, and our result shows that it is a smooth crossover from a finite slope to zero slope as temperature is increased. Finally, in this paper we concentrated on analytical predictions where several commonly used approximations were applied. Our results indicate that to completely explain all the anomalies in measured data of TMR, some further physical effects, which are neglected so far, may have to be included.

**Acknowledgments.** We gratefully acknowledge support by a RGC grant from the SAR Government of Hong Kong under grant number HKU 7115/98P, and a CRCG grant from the University of Hong Kong. H. G is supported by NSERC of Canada and FCAR of Québec. We thank the computer center of HKU for computational facilities.

## V. APPENDIX

In this appendix, we will derive the self-energy  $\Sigma_\alpha^r$ . For  $\alpha = L$ , the self-energy can be written rather easily<sup>21</sup>

$$(\Sigma_L^r)_{mn,\sigma\sigma'} = \sum_k T_{kLm}^* T_{kLn} g_{kL\sigma}^r \delta_{\sigma\sigma'}$$

where  $g_{k\alpha\sigma}^r$  is the free retarded Green's function for the lead  $\alpha$ . However, for  $\alpha = R$ , the situation becomes slightly complicated due to the spin-flip process. In the following, we will use the Dyson equation to calculate the self-energy function<sup>32</sup>. To facilitate the calculation, we will define the following retarded Green's functions,

$$G_{mn,\sigma\sigma'}^r(t_1, t_2) \equiv -i\theta(t_1 - t_2) \langle \{d_{m\sigma}(t_1), d_{n\sigma'}^+(t_2)\} \rangle \quad (32)$$

$$G_{kn,\sigma\sigma'}^r(t_1, t_2) \equiv -i\theta(t_1 - t_2) \langle \{C_{kR\sigma}(t_1), d_{n\sigma'}^+(t_2)\} \rangle \quad (33)$$

where  $m$  and  $n$  label the states in the quantum dot and  $k$  labels the states in the lead. To illustrate the calculation procedure, we consider  $G_{mn,\uparrow\uparrow}^r$  for simplicity. By using the Dyson equation

$$G^r = G_0^r + G_0^r \Sigma^r G^r \quad (34)$$

we obtain

$$\begin{aligned} G_{mn,\uparrow\uparrow}^r &= (G_0^r)_{mn,\uparrow\uparrow} + \sum_{k,m'} (G_0^r)_{mm',\uparrow\uparrow} \Sigma_{m'k,\uparrow\uparrow}^r G_{kn,\uparrow\uparrow}^r \\ &+ \sum_k (G_0^r)_{mm',\uparrow\uparrow} \Sigma_{m'k,\downarrow\uparrow}^r G_{kn,\downarrow\uparrow}^r \end{aligned} \quad (35)$$

Using the Dyson equation again for the retarded Green's functions  $G_{kn,\uparrow\uparrow}^r$  and  $G_{kn,\downarrow\uparrow}^r$ , we have the following relations

$$G_{kn,\uparrow\uparrow}^r = g_{kR\uparrow}^r \Sigma_{km,\uparrow\uparrow}^r G_{mn,\uparrow\uparrow}^r + g_{kR\uparrow}^r \Sigma_{km,\uparrow\downarrow}^r G_{mn,\downarrow\uparrow}^r \quad (36)$$

$$G_{kn,\downarrow\uparrow}^r = g_{kR\downarrow}^r \Sigma_{km,\downarrow\uparrow}^r G_{mn,\uparrow\uparrow}^r + g_{kR\downarrow}^r \Sigma_{km,\downarrow\downarrow}^r G_{mn,\downarrow\uparrow}^r \quad (37)$$

The self-energy matrix  $\Sigma^r$  has the following matrix elements from Eq.(9):  $(\Sigma^r)_{m'k,\uparrow\uparrow} = \cos(\theta/2)T_{kRm'}^*$ ,  $(\Sigma^r)_{m'k,\uparrow\downarrow} = -\sin(\theta/2)T_{kRm'}^*$ ,  $(\Sigma^r)_{m'k,\downarrow\uparrow} = \sin(\theta/2)T_{kRm'}^*$ ,  $(\Sigma^r)_{m'k,\downarrow\downarrow} = \cos(\theta/2)T_{kRm'}^*$ . From Eqs.(35), (36), and (37), we obtain

$$\begin{aligned} G_{mn,\uparrow\uparrow}^r &= (G_0^r)_{mn,\uparrow\uparrow} + \sum_{k,m'} (G_0^r)_{mm',\uparrow\uparrow} (\Sigma_R^r)_{m'k,\uparrow\uparrow} G_{n'n,\uparrow\uparrow}^r \\ &+ \sum_{k,m'} (G_0^r)_{mm',\uparrow\uparrow} (\Sigma_R^r)_{m'k,\downarrow\uparrow} G_{n'n,\downarrow\uparrow}^r \end{aligned} \quad (38)$$

with the corresponding self-energy functions  $(\Sigma_R^r)_{mn,\uparrow\uparrow}$  and  $(\Sigma_R^r)_{mn,\downarrow\uparrow}$  given by

$$\begin{aligned} (\Sigma_R^r)_{mn,\uparrow\uparrow} &= \sum_k T_{kRm}^* T_{kRn} [g_{kR\uparrow}^r \cos^2(\theta/2) \\ &+ g_{kR\downarrow}^r \sin^2(\theta/2)] \end{aligned} \quad (39)$$

$$(\Sigma_R^r)_{mn,\downarrow\uparrow} = \sum_k T_{kRm}^* T_{kRn} [g_{kR\downarrow}^r - g_{kR\uparrow}^r] \sin(\theta/2) \cos(\theta/2) \quad (40)$$

Similarly, we can obtain other self-energy functions

$$(\Sigma_R^r)_{mn,\downarrow\downarrow} = \sum_k T_{kRm}^* T_{kRn} [g_{kR\downarrow}^r - g_{kR\uparrow}^r] \sin(\theta/2) \cos(\theta/2) \quad (41)$$

$$\begin{aligned} (\Sigma_R^r)_{mn,\uparrow\downarrow} &= \sum_k T_{kRm}^* T_{kRn} [g_{kR\uparrow}^r \sin^2(\theta/2) \\ &+ g_{kR\downarrow}^r \cos^2(\theta/2)] \end{aligned} \quad (42)$$

Eqs.(39)-(42) are equivalent to Eq.(12).

<sup>1</sup> G.A. Prinz, Science, **282**, 1660 (1998).

<sup>2</sup> M. Baibich *et.al.*, Phys. Rev. Lett. **61**, 2472 (1988).

<sup>3</sup> For a review see, R. Meservey and P.M. Tedrow, Phys. Rep. **238**, 173 (1994).

<sup>4</sup> D.J. Monsma, J.C. Lodder, Th.J.A. Popma, and B. Diény, Phys. Rev. Lett. **74**, 5260 (1995); D.J. Monsma, R. Vlutters, J.C. Lodder, Science, **281**, 407 (1998).

<sup>5</sup> S. Egger, C.H. Back, J. Krewer and D. Pescia, Phys. Rev. Lett. **83**, 2833 (1999).

<sup>6</sup> M. Dax, Semicond. Int. **20**, 84 (1997).

<sup>7</sup> M. Julliere, Phys. Lett. A **54**, 225 (1975).

<sup>8</sup> J.S. Moodera, L.R. Kinder, T.M. Wong, and R. Meservey, Phys. Rev. Lett. **74**, 3273 (1995).

<sup>9</sup> J.C. Slonczewski, Phys. Rev. B **39**, 6995 (1989).

<sup>10</sup> J.S. Moodera, J. Nowak and R.J.M. van de Veerdonk, Phys. Rev. Lett. **80**, 2941 (1998).

<sup>11</sup> X. Zhang *et.al.*, Phys. Rev. B **56**, 5484 (1997).

<sup>12</sup> A.M. Bratkovsky, Phys. Rev. B **56**, 2344 (1997).

<sup>13</sup> J. Barnaś and A. Fert, Phys. Rev. Lett. **80**, 1058 (1998).

<sup>14</sup> S. Zhang, P.M. Levy, A.C. Marley and S.S.P. Parkin, Phys. Rev. Lett. **79**, 3744 (1997).

<sup>15</sup> J. Inoue and S. Maekawa, Phys. Rev. B **53**, R11927 (1996).

<sup>16</sup> J.M. MacLaren, X.-G. Zhang and W. H. Butler, Phys. Rev. B **56**, 11827 (1997).

<sup>17</sup> J. Mathon, Phys. Rev. B **56**, 11810 (1997).

<sup>18</sup> L. Sheng, Y. Chen, H.Y. Teng, and C.S. Ting, Phys. Rev. B **59**, 480 (1999).

<sup>19</sup> M. Büttiker, J. Phys. Condens. Matter **5**, 9361 (1993).

<sup>20</sup> N.N. Bogoliubov, J. Phys. USSR, **11**, 23(1947).

<sup>21</sup> A.P. Jauho, N.S. Wingreen, and Y. Meir, Phys. Rev. B **50**, 5528(1994).

<sup>22</sup> S. Datta, *Electronic Transport in Mesoscopic Systems*, (Cambridge University Press, New York, 1995).

<sup>23</sup> M. P. Anantram and S. Datta, Phys. Rev. B **51**, 7632 (1995).

<sup>24</sup> C.A. Stafford, Phys. Rev. Lett. **77**, 2770 (1996).

<sup>25</sup> J. Wang, *et. al.*, Phys. Rev. Lett **80**, 4277 (1998).

<sup>26</sup> T. Christen and M. Büttiker, Phys. Rev. Lett. **77**, 143 (1996).

<sup>27</sup> M. H. Pedersen and M. Büttiker, Phys. Rev. B **58**, 12993 (1998).

<sup>28</sup> Z.S. Ma, J. Wang and H. Guo, Phys. Rev. B **57**, 9108 (1998); Phys. Rev. B **59**, 7575 (1999).

<sup>29</sup> B.G. Wang, J. Wang, and H. Guo, to appear in J. Appl. Phys. 1999.

<sup>30</sup> Here we have used the Thomas-Fermi approximation.

<sup>31</sup> T. Christen and M. Büttiker, Europhys. Lett. **35**, 523 (1996).

<sup>32</sup> C. Caroli, *et.al.*, J. Phys. C **4**, 916 (1971); S. Hershfield, J. H. Davies, and J. W. Wilkins, Phys. Rev. B **46**, 7046 (1992).

fixed at  $v = 2$ . The other parameters are the same as those of Fig.(1).

Fig. (3) The TMR ratio versus the voltage. Solid line  $\beta = \infty$  and dotted line  $\beta = 1$ . The other parameters are the same as those of Fig.(1).

Fig. (4) The second order nonlinear conductance  $G_{111}$ , which is the slope of conductance at zero bias, versus temperature parameter  $\beta$ . Other parameters:  $\Gamma_{1\uparrow} = 1.0$ ,  $\Gamma_{1\downarrow} = 0.4$ ,  $\Gamma_{2\uparrow} = 0.8$ ,  $\Gamma_{2\downarrow} = 0.2$ ,  $E_F = 2.5$ , and  $E_0 = 3$ .

## FIGURE CAPTIONS

Fig. (1) (a). The current  $I$  versus the voltage for different orientation angles:  $\theta = 0$  (solid line),  $\theta = 0.4\pi$  (dotted line),  $\theta = 0.8\pi$  (dashed line). Inset: the schematic plot showing the TMR device considered in this work. (b). The current  $I$  versus orientation  $\theta$  at different bias  $v = 2, 5, 8, 11, 14$ . Other parameters:  $\Gamma_{\uparrow} = 1.0$ ,  $\Gamma_{\downarrow} = 0.4$ ,  $C_1 = C_2 = 0.5$ ,  $E_F - E_0 = -2$ , and  $\hbar = e = 2m = 1$ .

Fig. (2) The current  $I$  versus the orientation  $\theta$  at different temperatures:  $\beta = 1$  (solid line),  $\beta = 0.5$  (dotted line)  $\beta = 0.2$  (dashed line). Here the voltage is

Fig1 a.

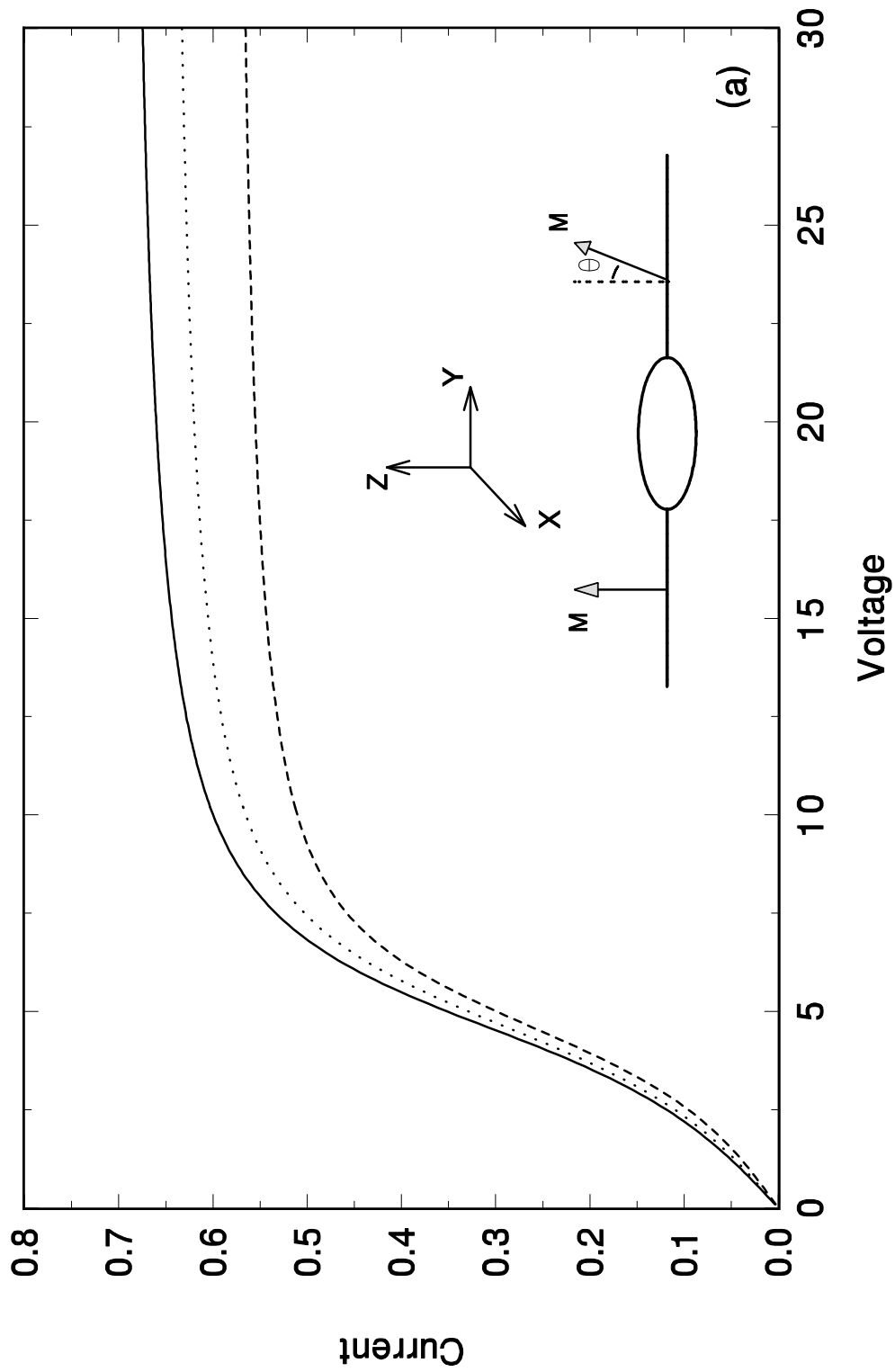


Fig1b.

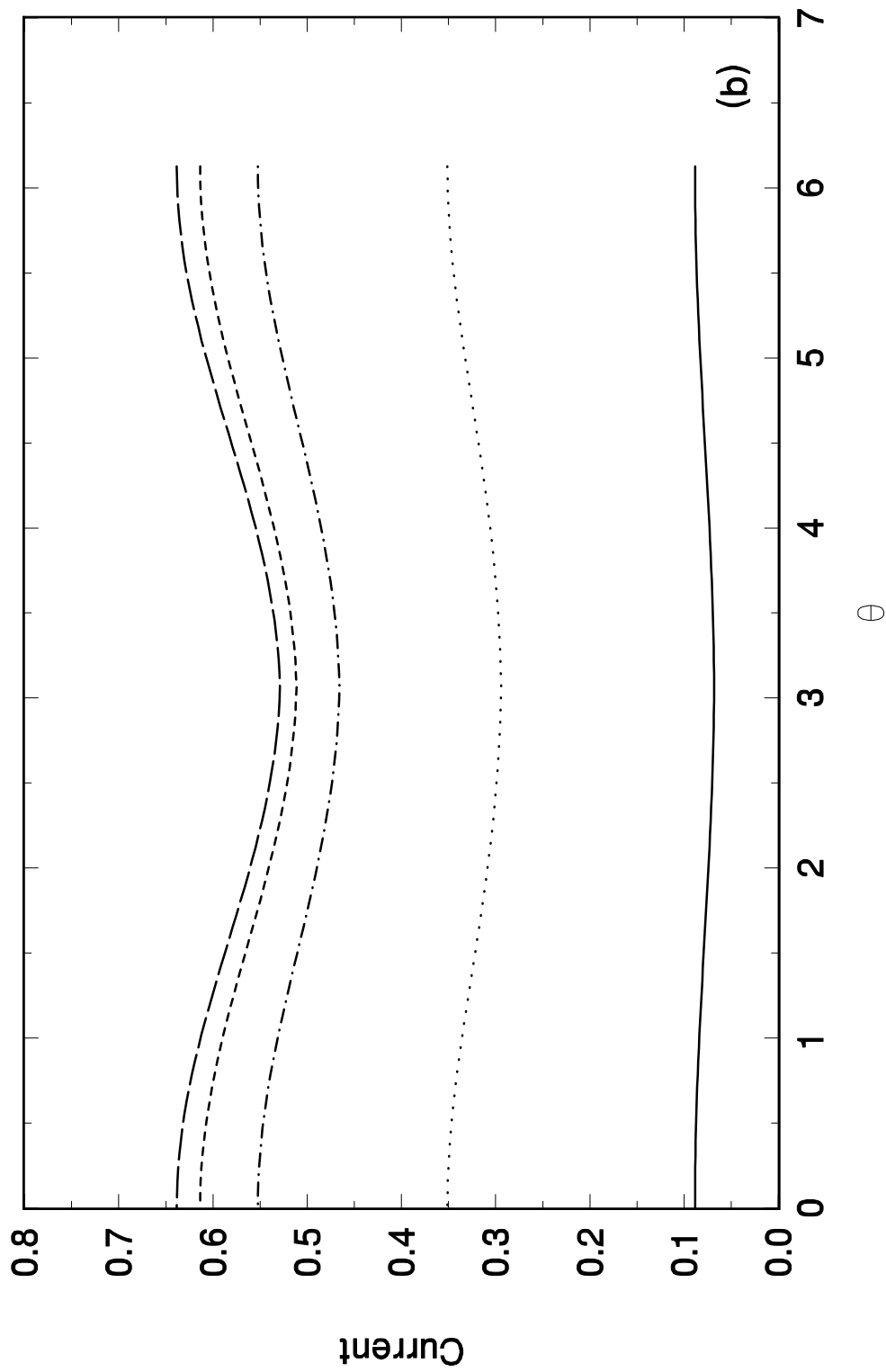


Fig2

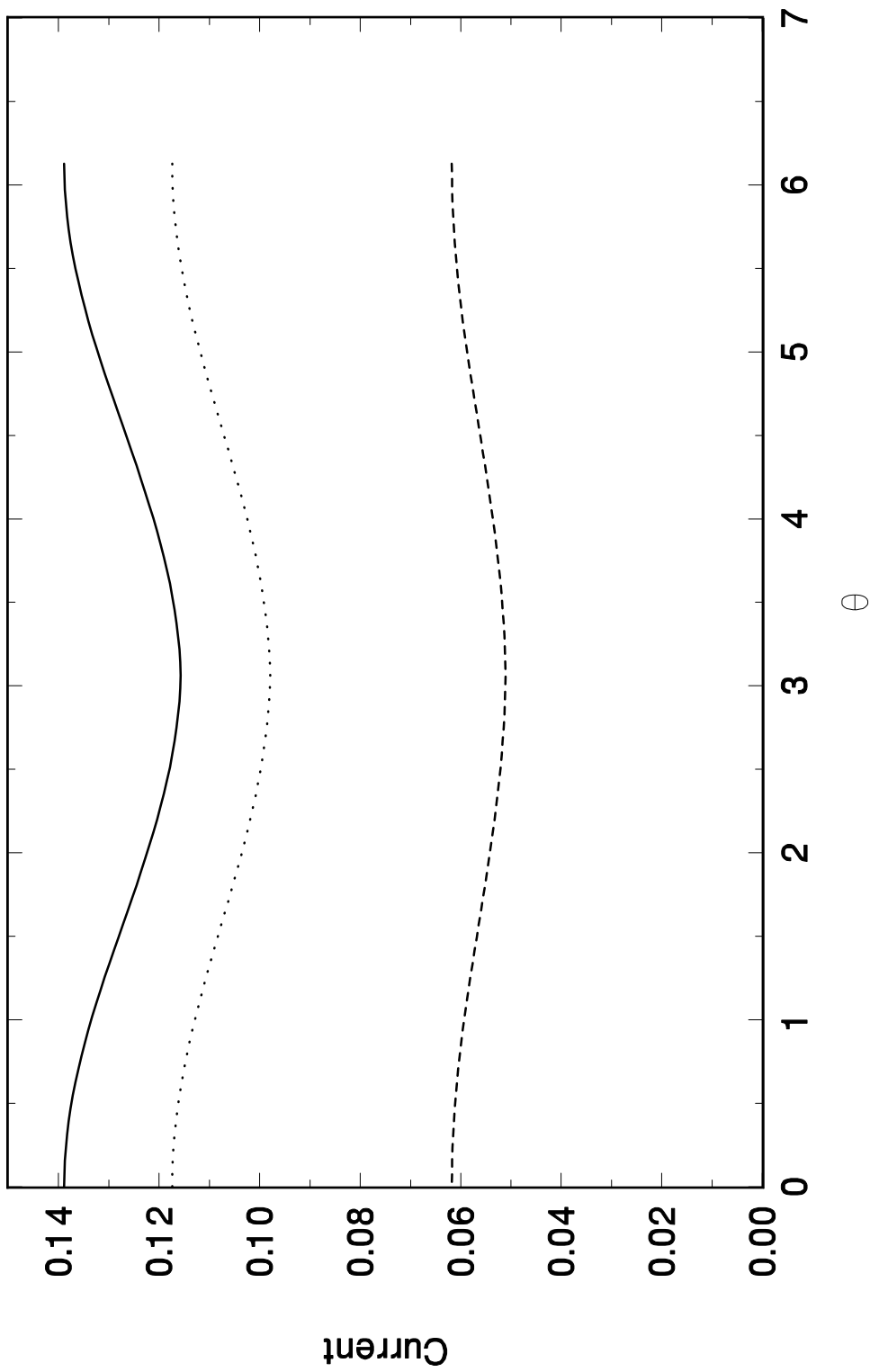


Fig3.

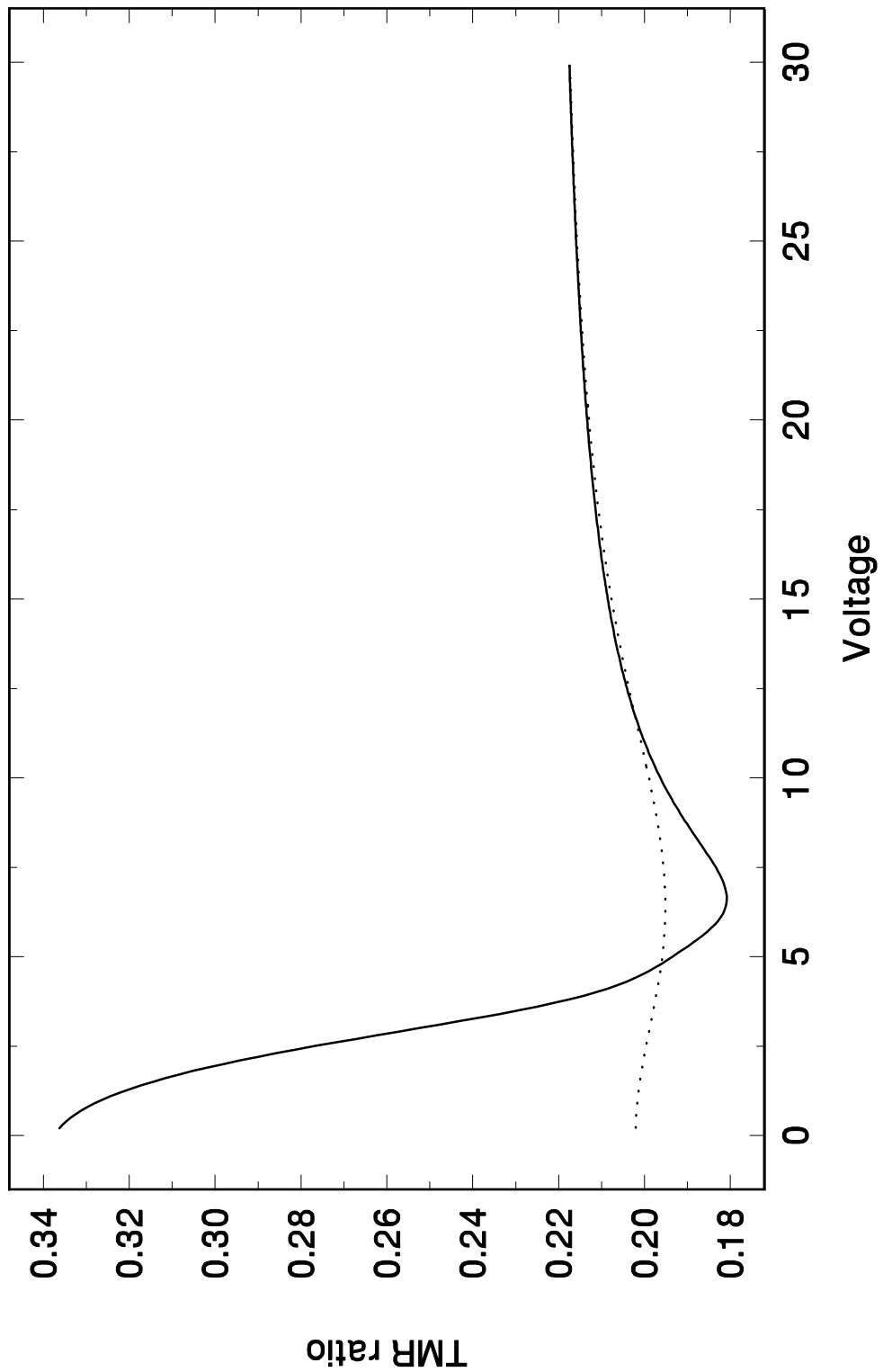


Fig4.

